



Research paper

Numerical separation of the front-side attack and double-inversion retention pathways of S_N2 reactions

Paszkál Papp, Viktor Tajti, Gábor Czakó*

MTA-SZTE Lendület Computational Reaction Dynamics Research Group, Interdisciplinary Excellence Centre and Department of Physical Chemistry and Materials Science, Institute of Chemistry, University of Szeged, Rerrich Béla tér 1, Szeged H-6720, Hungary

A B S T R A C T

We describe a vector-projection method to identify inversion and retention mechanisms in S_N2 reactions and a transition state (TS) attack-angle-based approach allowing the separation of the front-side attack and double-inversion retention trajectories by following the leaving group backwards to the TS regions characterized by attack angles of 40–100° and 120–180°, respectively. The methods are tested for the F[−] + CH₃Cl/CH₃I S_N2 reactions, revealing that double inversion is the dominant retention mechanism at low collision energies and the time-based separation of the front-side attack (fast, direct) and double-inversion (slow, indirect) pathways is only unambiguous for F[−] + CH₃Cl.

1. Introduction

Bimolecular nucleophilic substitution (S_N2) is probably the best-known stereo-specific reaction type in organic chemistry. The back-side attack Walden-inversion mechanism of S_N2 reactions is a major topic in every organic chemistry class at universities. The front-side attack retention pathway is less-known, but one can read about the atomic-level mechanisms of both stereo-specific pathways in the book of Ingold published in the early 1950s [1]. In the past couple of decades several experimental and theoretical studies investigated the dynamics of S_N2 reactions showing that the Walden-inversion mechanism is quite complex involving ion-dipole, hydrogen-bonded, and halogen-bonded (front-side) complex formations as well as rebound, stripping, and roundabout mechanisms [2–11]. However, as far as stereo-specificity is concerned, only two major pathways, Walden inversion and front-side attack retention, were known until 2015, when our reaction dynamics simulations revealed a double-inversion retention pathway for the F[−] + CH₃Cl S_N2 reaction [12]. The first step of double inversion is a proton-abstraction induced inversion via a FH···CH₂Cl[−] double-inversion transition state (DITS) followed by a second inversion through the usual Walden-inversion TS (WaldenTS) as shown in Fig. 1. The two inversions result in retention of the initial configuration. Later we found DITSs for many S_N2 reactions such as X[−] + CH₃Y, where X = F, Cl, Br, I, OH, SH, CN, NH₂, PH₂ and Y = F, Cl, Br, I as well as F[−] + CH₃CH₂Cl [13–16]. In 2017 Hase and co-workers showed that double inversion is a non-intrinsic-reaction-coordinate process, where DITS plays a major role [17]. Wang and co-workers [18,19] identified double inversion in aqueous solutions and our *ab initio* study also found double-inversion

pathways for the micro-hydrated F[−](H₂O) + CH₃I S_N2 reaction [20]. Furthermore, double-inversion-type mechanisms were recently revealed for N-centered S_N2 reactions, as well [21,22].

We could reveal double inversion due to two key reasons: (1) We developed an analytical potential energy surface for the F[−] + CH₃Cl S_N2 reaction allowing to compute millions of trajectories, thereby uncovering low-probability reaction pathways [12]. (2) We implemented a numerical technique which identified products retaining the initial configuration [12]. Animations of the retention trajectories, found at collision energies below the front-side attack barrier height, revealed the new double-inversion reaction pathway [12]. Now the question comes how to distinguish between the front-side attack and double-inversion retention pathways *numerically*? On the basis of many trajectory animations we found that front-side attack is a fast direct process, whereas double inversion is indirect proceeding slowly [12]. Thus, based on integration time, we could separate the front-side attack and double-inversion pathways. This technique worked well for the F[−] + CH₃Cl and F[−] + CH₃F reactions [12,23]; however, for F[−] + CH₃I we found some double-inversion trajectories with shorter time than that of the front-side attack ones [24]. Thus, in the case of the F[−] + CH₃I S_N2 reaction, we just reported the total retention cross sections without mechanism-specific separation [24]. Here, we develop a methodology allowing numerical separation of the front-side attack and double-inversion pathways, thereby checking the validity of our previous time-based assignments [12] and providing separate double-inversion and front-side attack cross sections for the first time for the F[−] + CH₃I reaction. The methodological and computational details are described in Section 2, the results are presented and

* Corresponding author.

E-mail address: gczako@chem.u-szeged.hu (G. Czakó).

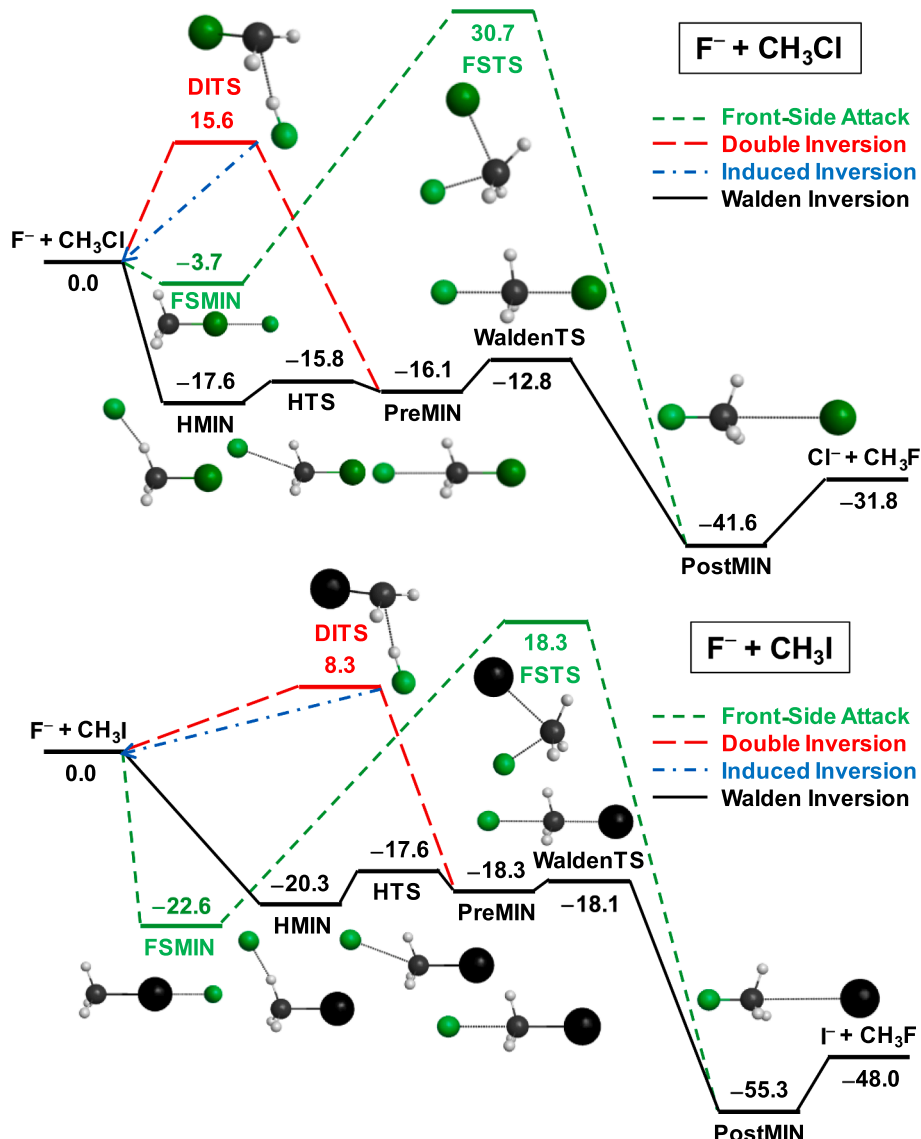


Fig. 1. Different pathways of the $\text{F}^- + \text{CH}_3\text{Cl}$ and $\text{F}^- + \text{CH}_3\text{I}$ $\text{S}_{\text{N}}2$ reactions, showing the stationary-point structures and classical relative energies (kcal/mol) corresponding to the analytical PESs [12,24]. Data are taken from Ref. [12] (Ref. [29] for FFSMIN) and Ref. 24 for $\text{F}^- + \text{CH}_3\text{Cl}$ and $\text{F}^- + \text{CH}_3\text{I}$, respectively.

discussed in Section 3, and the letter ends with summary and conclusions in Section 4.

2. Methods and computational details

2.1. Separating inversion and retention with a vector-projection method

The first step of the stereo-specific trajectory analysis is to determine the configuration of the products relative to that of the reactants, thereby distinguishing between inversion and retention pathways. Previously we applied an Eckart-transformation-based method [25,26] to relate the product configuration to a reference structure by a pseudo-rotational matrix, whose determinant shows if inversion or retention occurs [12]. Here, we present a more practical method to determine the relative configurations of the product molecules. Let us consider a product molecule with a tetrahedral CXYZU group, where C denotes a central atom, usually a carbon atom, and X, Y, Z, and U are atoms connecting to C. For example, in the case of the CH_3F , CH_3OH , and $\text{CH}_3\text{CH}_2\text{F}$ products $\{X, Y, Z, U\}$ may be chosen as $\{\text{H}, \text{H}, \text{H}, \text{F}\}$, $\{\text{H}, \text{H}, \text{H}, \text{O}\}$, and $\{\text{H}, \text{H}, \text{C}, \text{F}\}$, respectively. Note that the results are not sensitive to the choice of labeling the atoms by X, Y, Z, and U. Now let

us define the following vectors:

$$\mathbf{r}_{CX} = \mathbf{r}_X - \mathbf{r}_C \quad (1)$$

$$\mathbf{r}_{CY} = \mathbf{r}_Y - \mathbf{r}_C \quad (2)$$

$$\mathbf{r}_{CZ} = \mathbf{r}_Z - \mathbf{r}_C \quad (3)$$

$$\mathbf{r}_{CU} = \mathbf{r}_U - \mathbf{r}_C \quad (4)$$

where \mathbf{r}_C , \mathbf{r}_X , \mathbf{r}_Y , \mathbf{r}_Z , and \mathbf{r}_U , denote the Cartesian coordinates of the C, X, Y, Z, and U atoms of the product, respectively. Using the above vectors we can calculate

$$\mathbf{n}_{CZU} = \mathbf{r}_{CZ} \times \mathbf{r}_{CU}, \quad (5)$$

$$s_X = \mathbf{r}_{CX} \cdot \mathbf{n}_{CZU}, \quad (6)$$

$$s_Y = \mathbf{r}_{CY} \cdot \mathbf{n}_{CZU}, \quad (7)$$

where \mathbf{n}_{CZU} is a normal vector of the CZU plane and s_X and s_Y are projections of the \mathbf{r}_{CX} and \mathbf{r}_{CY} vectors onto the \mathbf{n}_{CZU} vector, respectively, as shown in Fig. 2. If the sign of $s_X - s_Y$ is found to be the same/opposite as that of the corresponding quantity in the reactant, retention/inversion occurred. Here, two notes are in order. First, the reactant configuration is the same for every trajectory, thus, the sign of $s_X - s_Y$ needs to be considered only once in the case of the reactant molecule. Second, s_X

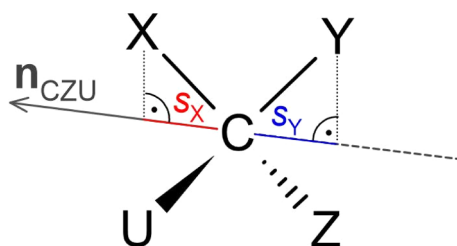


Fig. 2. Graphical representation of the vector-projection method. For the sake of simplicity s_X and s_Y correspond to normalized n_{CZU} . Red and blue denote positive and negative values, respectively.

and s_Y usually have opposite signs; thus, the sign of $s_X - s_Y$ is the same as that of s_X . However, in a highly distorted product molecule, the X and Y atoms may present at the same side of the CZU plane, resulting in two positive or two negative values for s_X and s_Y . In these very rare events, the assignments based on s_X or s_Y only may become incorrect, whereas the $s_X - s_Y$ handles correctly this situation as well. One may also apply the above vector-projection method for the “non-reactive” trajectories, which may reveal inverted reactants via the so-called induced-inversion [12] pathway. In the induced-inversion channel, the first step of double inversion, i.e., the proton abstraction induced inversion, is not followed by substitution, thereby resulting in an inverted reactant.

2.2. Separating front-side attack and double inversion with transition-state attack angles

After separating inversion and retention mechanisms, the next challenge is to numerically distinguish between front-side attack and double-inversion retention pathways. The first intuition suggests that one should identify the first inversion via DITS, thereby defining double inversion. However, hydrogen-bonded complex formation and partial proton abstraction often occur in S_N2 reactions, thus we found that many trajectories visit DITS-like configurations even in the case of Walden inversion [27]. Therefore, the DITS-based identification of the double-inversion pathway does not seem promising. Here, we introduce a different approach to separate front-side attack and double inversion, which is about to capture the second, Walden-inversion step of double inversion. The idea is that retention trajectories which end via WaldenTS correspond to double inversion, whereas the ones going through the front-side attack TS (FSTS) belong to the front-side attack pathway. Let us consider a general S_N2 reaction $X^- + R_1R_2CHY \rightarrow R_1R_2CHX + Y^-$, where X,Y = F, Cl, Br, I, OH, etc. and R₁,R₂ = H, CH₃, etc. The key behind the above idea is that at WaldenTS and FSTS the

C–Y distance is similar, but the X–C–Y angle is 180° or close to 180° for WaldenTS and 80–90° for FSTS (see Fig. 1). We follow the C–Y distance backwards from the end of the trajectory and define a TS attack angle (γ) as the X–C–Y angle at the point where the C–Y distance passes a predefined TS value. The values of γ are around 180° and 80° for double-inversion and front-side attack trajectories, respectively. Thus, using a dividing angle of about 110°, one can separate the double-inversion and front-side attack retention pathways.

2.3. Computational details

Quasi-classical trajectory (QCT) computations are performed for the $F^- + CH_3Cl$ and $F^- + CH_3I$ S_N2 reactions using *ab initio* analytical potential energy surfaces (PESs) [12,24]. The vibrational ground states of the reactants are prepared using standard normal mode sampling [28]. The initial orientations of the reactants are randomly sampled and the center-of-mass distance of the reactants is $(x^2 + b^2)^{1/2}$, where $x = 20$ bohr and b is the impact parameter, which is scanned from 0 to b_{max} with a step of 1 bohr, unless otherwise noted. Trajectories are run at collision energies (E_{coll}) of 10, 15, 20, 30, 40, 50, and 60 kcal/mol and 5000 trajectories are computed at each b at a given E_{coll} . To obtain improved statistics we use a smaller b step of 0.25 bohr at $E_{coll} = 50$ and 60 kcal/mol for the computation of the γ and time distributions. We use an integration step of 0.0726 fs (3 atomic time unit), record geometries at every 10th step, and propagate trajectories until the maximum of the inter-atomic distances becomes 1 bohr larger than the initial one. Retention and induced-inversion trajectories are identified using the vector-projection method described above. TS attack angles are determined at C–Cl and C–I distances of 2.4 and 2.7 Å, respectively. Front-side attack and double inversion are defined for γ less and greater than 111°, respectively.

3. Results and discussions

The schematic PESs of the $F^- + CH_3Cl/CH_3I$ S_N2 reactions introducing the different reaction pathways are shown in Fig. 1. As seen, both reactions are highly exothermic and their Walden-inversion mechanisms involve several submerged minima and transition states. The retention pathways have positive barriers and the double-inversion barrier heights are about half of the corresponding front-side attack barriers. Furthermore, in the case of the iodine leaving group the retention barrier heights are again about half of the corresponding barriers of the $F^- + CH_3Cl$ reaction. Thus, stationary-point energetics suggests that double-inversion opens a lower-energy retention pathway than front-side attack, and retention may be more significant in

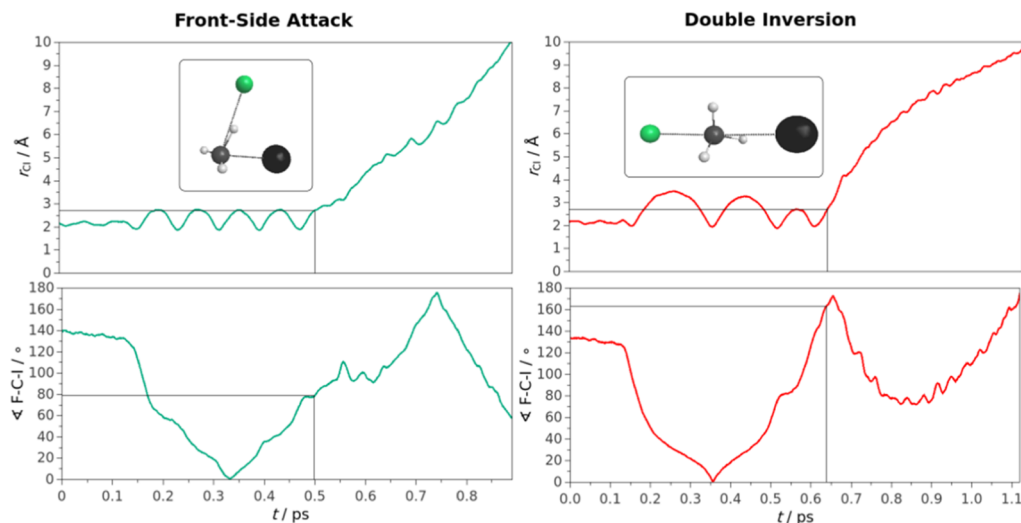


Fig. 3. C–I distances and F–C–I angles as a function of time for representative front-side attack and double-inversion trajectories demonstrating the reaction-pathway assignments for the $F^- + CH_3I$ reaction. The trajectory frames are shown at C–I distance of 2.7 Å and the front-side attack or double-inversion assignment is based on the corresponding F–C–I angle being less or greater than 111°, respectively.

$\text{F}^- + \text{CH}_3\text{I}$ than in the case of the $\text{F}^- + \text{CH}_3\text{Cl}$ reaction.

Fig. 3 exemplifies the reaction-pathway assignments for a front-side attack and a double-inversion $\text{F}^- + \text{CH}_3\text{I}$ retention trajectory. Following the C–I distance and the F–C–I angle from the final configuration backwards in time, one can see that the C–I distance decreases almost monotonically, whereas the time dependence of the F–C–I angle is less predictable due to the fact that $\text{I}^- \cdots \text{H}_3\text{CF}$ may have large amplitude bending/torsional motions and CH_3F may rotate in the exit channel. When the C–I distance passes 2.7 Å we can read the TS attack angle, which is 79° and 163° for the left and right panels of Fig. 3, respectively. Based on these angles, one can assign the trajectories to the front-side attack (left) and double-inversion (right) pathways. Once the C–I bond is formed the C–I distance oscillates between 2 and 3 Å, while the F–C–I angle may vary significantly because F^- or the HF unit may roam around CH_3I or CH_2I^- , respectively. In the present examples, the F–C–I angle approaches zero, as seen in Fig. 3, which is not surprising because the $\text{F}^- \cdots \text{ICH}_3$ front-side complex (FSMIN in Fig. 1) is the deepest minimum in the entrance channel of the $\text{F}^- + \text{CH}_3\text{I}$ reaction. Our previous QCT simulations revealed that front-side complex formation is significant in the $\text{F}^- + \text{CH}_3\text{I}$ reaction, whereas negligible in $\text{F}^- + \text{CH}_3\text{Cl}$ [29]. Furthermore, nearly zero F–C–I angle can also form when the HF fragment moves around CH_2I^- during the double-inversion process. In the first 0.1 ps the F–C–I angle is nearly constant, because at the beginning of the reaction the interaction between the reactants is weak and the rotational angular momentum of CH_3I is set to zero.

The TS attack angle distributions for the retention channels of the $\text{F}^- + \text{CH}_3\text{Cl}/\text{CH}_3\text{I}$ $\text{S}_{\text{N}}2$ reactions at different collision energies are

shown in Fig. 4. At $E_{\text{coll}} = 30$ kcal/mol the distributions are in the 120–180° range peaking at around 180° and 150° for $\text{F}^- + \text{CH}_3\text{Cl}$ and $\text{F}^- + \text{CH}_3\text{I}$, respectively. This finding shows that at $E_{\text{coll}} = 30$ kcal/mol all the retention trajectories proceed via the double-inversion pathway. At larger collision energies of 50 and 60 kcal/mol, the TS attack angle distributions become bimodal, peaking around 60–80° and 140–160° corresponding to front-side attack and double inversion, respectively. The distributions are nearly zero between the two peaks around 110°, especially for $\text{F}^- + \text{CH}_3\text{Cl}$, allowing separation of the two different retention pathways. Thus, as seen in Fig. 4, using a dividing angle of 111°, one can almost unambiguously assign trajectories to front-side attack and double inversion with only a few % uncertainties. At low collision energies clearly double inversion dominates and the front-side attack peak emerges as collision energy increases.

Once we separate the front-side attack and double-inversion pathways based on the TS attack angles, we can plot the mechanism-specific retention and induced-inversion cross sections as a function of collision energy as shown in Fig. 5. At low collision energies all the retention products are formed via double inversion and the front-side attack pathway opens at collision energies of 40–50 and 30 kcal/mol for $\text{F}^- + \text{CH}_3\text{Cl}$ and $\text{F}^- + \text{CH}_3\text{I}$ reactions, respectively. The double-inversion cross sections increase with collision energy, peak at 30/20 kcal/mol for $\text{F}^- + \text{CH}_3\text{Cl}/\text{CH}_3\text{I}$ and then decrease with increasing E_{coll} . This finding can be explained by the fact that double inversion is an indirect process which cannot be activated by additional collision energy. Furthermore, at E_{coll} of 30/20 kcal/mol the proton-abstraction channels leading to $\text{HF} + \text{CH}_2\text{Cl}^-/\text{CH}_2\text{I}^-$ open [12,24] on the expense of double inversion, because the HF fragment may depart

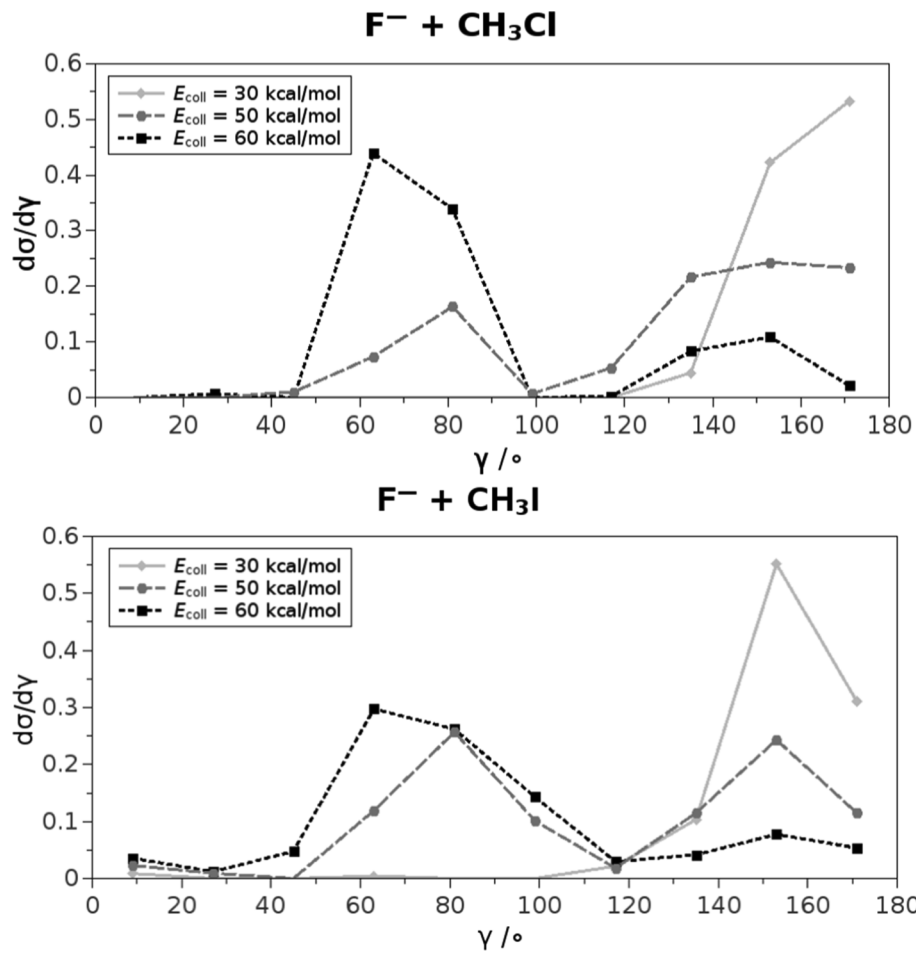


Fig. 4. Normalized transition-state attack angle distributions for the retention channels of the $\text{F}^- + \text{CH}_3\text{Cl}$ and $\text{F}^- + \text{CH}_3\text{I}$ $\text{S}_{\text{N}}2$ reactions at different collision energies.

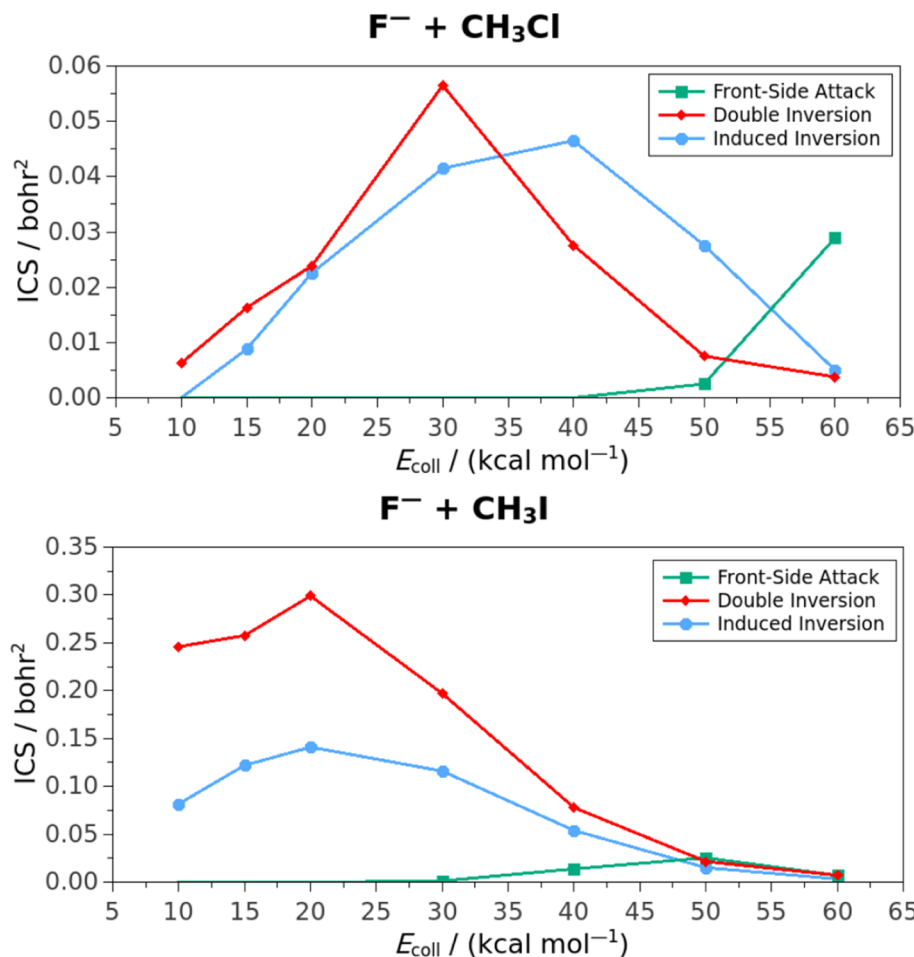


Fig. 5. Mechanism-specific cross sections for the retention and induced-inversion channels of the $\text{F}^- + \text{CH}_3\text{Cl}$ and $\text{F}^- + \text{CH}_3\text{I}$ S_2N reactions as a function of collision energy.

before induced inversion, the first step of double inversion could occur. The collision energy dependence of the induced-inversion, which results in an inverted $\text{CH}_3\text{Cl}/\text{CH}_3\text{I}$, cross sections is similar to that of double inversion. Induced- and double-inversion cross sections have similar magnitudes, though induced inversion is clearly more dominant than double inversion at 40–50 kcal/mol in the case of $\text{F}^- + \text{CH}_3\text{Cl}$, whereas double inversion has about twice as large cross sections than induced inversion in $\text{F}^- + \text{CH}_3\text{I}$. Thus, in the more indirect $\text{F}^- + \text{CH}_3\text{I}$ reaction the induced inversion is more likely followed by a reactive substitution even than in the case of the $\text{F}^- + \text{CH}_3\text{Cl}$ system. At low collision energies the double- and induced-inversion reactivity of the $\text{F}^- + \text{CH}_3\text{I}$ reaction is significantly higher, usually by an order of magnitude, than that of the $\text{F}^- + \text{CH}_3\text{Cl}$ reaction, in accord with the lower barrier for the former system.

In our previous studies we separated double inversion from front-side attack based on integration time in the case of the $\text{F}^- + \text{CH}_3\text{Cl}$ reaction [12]; here, we can validate our previous work by computing the time distributions for the front-side attack and double-inversion trajectories. As Fig. 6 shows, in the case of $\text{F}^- + \text{CH}_3\text{Cl}$ almost all the front-side attack trajectories finish in the first bin having 0.726 ps size, whereas double inversion has a broad time distribution in the 1–7 ps range and negligible trajectories finish within 0.726 ps. Therefore, the front-side attack and double-inversion pathways of the $\text{F}^- + \text{CH}_3\text{Cl}$ reaction can be unambiguously separated based on integration time, validating our previous studies where we used a 0.65 ps time limit for front-side attack [12]. In the case of the $\text{F}^- + \text{CH}_3\text{I}$ reaction the picture is not so clear; because front-side attack is less direct, resulting in overlapping time distributions as shown in Fig. 6. Front-side attack is

still more direct than double inversion, about 70% of the front-side attack trajectories finish within 0.726 ps, whereas virtually no double inversion completes within this short time frame. However, about 20% of the front-side attack and also about 20% of the double-inversion trajectories finish in the same 0.726–1.452 ps time range, making the unambiguous time-based separation of the $\text{F}^- + \text{CH}_3\text{I}$ retention pathways impossible. This conclusion is in agreement with our previous finding based on visual inspections of several trajectory animations [24]. This was the reason why we did not report mechanism-specific retention cross sections for the $\text{F}^- + \text{CH}_3\text{I}$ reaction in our previous studies [24,30], before the development of present TS attack angle separation method.

4. Summary and conclusions

Since the discovery of the double-inversion mechanism for S_2N reactions in 2015 [12], a general, numerical method has not been developed to separate the double-inversion and front-side attack retention pathways. Here we have presented such an approach based on the idea that the second inversion of the double-inversion process, which goes via a Walden-inversion TS, should be identified and distinguished from the front-side attack TS using transition-state attack angles defined by following trajectories backwards and finding the point where the TS region is reached. We show that the TS attack angle distributions are bimodal featuring two peaks at 40–100° and 120–180° corresponding to front-side attack and double inversion, respectively, thereby allowing unambiguous reaction-pathway assignment with only a few % uncertainties. We demonstrate the performance of the above approach by

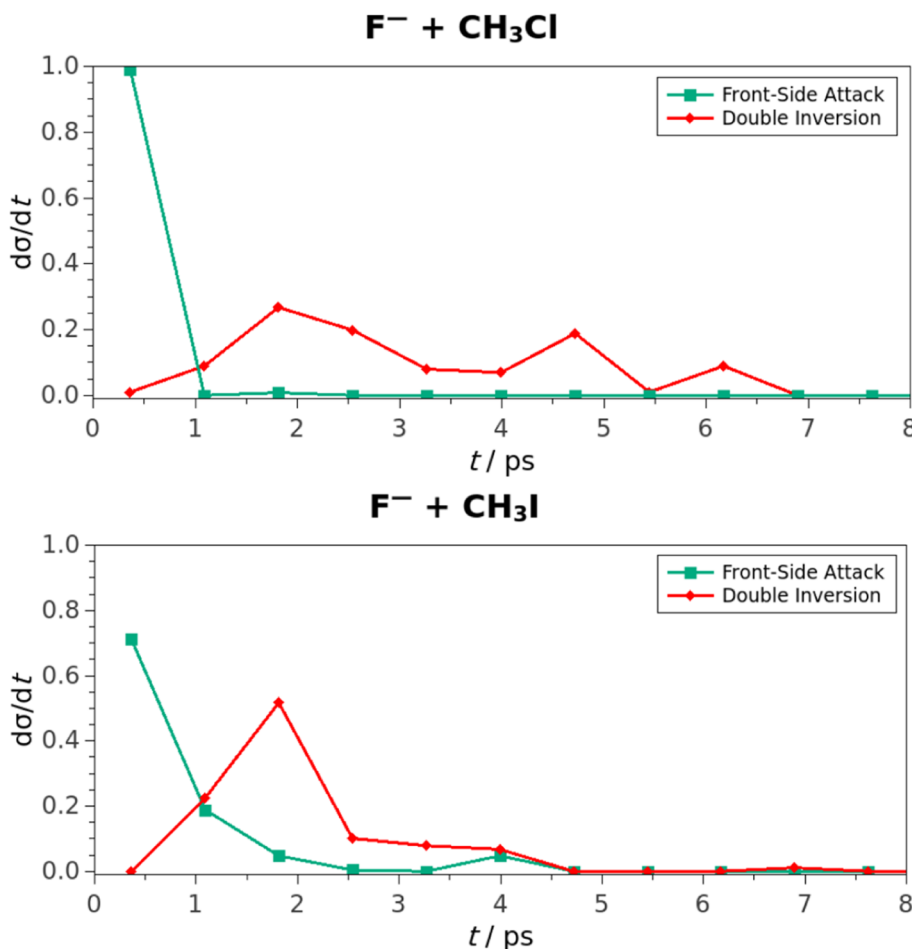


Fig. 6. Normalized integration time distributions for the front-side attack and double-inversion trajectories of the $\text{F}^- + \text{CH}_3\text{Cl}$ and $\text{F}^- + \text{CH}_3\text{I}$ $\text{S}_{\text{N}}2$ reactions at collision energy of 60 kcal/mol.

computing mechanism-specific retention cross sections for the $\text{F}^- + \text{CH}_3\text{Cl}$ and $\text{F}^- + \text{CH}_3\text{I}$ $\text{S}_{\text{N}}2$ reactions, for the first time in the case of the latter. Double inversion is found to be the dominant retention pathway at low collision energies having significantly larger cross sections in the case of the iodine leaving group. Integration time distributions reveal that front-side attack is fast and double inversion is slow allowing their unambiguous separation in the case of the $\text{F}^- + \text{CH}_3\text{Cl}$ reaction, whereas about 30% of the $\text{F}^- + \text{CH}_3\text{I}$ front-side attack trajectories are indirect with similar timescale as double inversion, hampering the time-based reaction-path assignment for the $\text{F}^- + \text{CH}_3\text{I}$ system.

Besides the TS attack-angle-based reaction pathway assignment technique, we also introduce a practical method to determine the relative configuration of the products using vector projection, thereby numerically identifying inversion and retention mechanisms. This vector-projection approach is more straightforward than the Eckart transformation-based method [25,26] used previously [12,23,24,30] in our group. The present techniques may become useful tools to perform stereo-specific quasi-classical trajectory analysis for $\text{S}_{\text{N}}2$ reactions.

CRediT authorship contribution statement

Paszkál Papp: Software, Validation, Formal analysis, Investigation, Data curation, Visualization. **Viktor Tajti:** Conceptualization, Methodology. **Gábor Czakó:** Conceptualization, Methodology, Validation, Resources, Writing - original draft, Writing - review & editing, Supervision, Project administration, Funding acquisition.

Declaration of Competing Interest

The authors declare that they have no known competing financial interests or personal relationships that could have appeared to influence the work reported in this paper.

Acknowledgements

We thank the National Research, Development and Innovation Office–NKFIH, K-125317, the Ministry of Human Capacities, Hungary grant 20391-3/2018/FEKUSTRAT, and the Momentum (Lendület) Program of the Hungarian Academy of Sciences for financial support.

References

- [1] C.K. Ingold, Structure and Mechanisms in Organic Chemistry, Cornell Univ. Press, Ithaca, NY, 1953.
- [2] L.A. Angel, K.M. Ervin, J. Phys. Chem. A 105 (2001) 4042.
- [3] J. Mikosch, S. Trippel, C. Eichhorn, R. Otto, U. Lourderaj, J.-X. Zhang, W.L. Hase, M. Weidemüller, R. Wester, Science 319 (2008) 183.
- [4] J.I. Brauman, Science 319 (2008) 168.
- [5] J. Zhang, J. Mikosch, S. Trippel, R. Otto, M. Weidemüller, R. Wester, W.L. Hase, J. Phys. Chem. Lett. 1 (2010) 2747.
- [6] J. Mikosch, J. Zhang, S. Trippel, C. Eichhorn, R. Otto, R. Sun, W.A. de Jong, M. Weidemüller, W.L. Hase, R. Wester, J. Am. Chem. Soc. 135 (2013) 4250.
- [7] P. Manikandan, J. Zhang, W.L. Hase, J. Phys. Chem. A 116 (2012) 3061.
- [8] J. Xie, R. Otto, J. Mikosch, J. Zhang, R. Wester, W.L. Hase, Acc. Chem. Res. 47 (2014) 2960.
- [9] J. Xie, W.L. Hase, Science 352 (2016) 32.
- [10] I. Szabó, G. Czakó, J. Phys. Chem. A 121 (2017) 9005.
- [11] G. Czakó, T. Györi, B. Olasz, D. Papp, I. Szabó, V. Tajti, D.A. Tasi, Phys. Chem. Chem. Phys. 22 (2020) 4298.

- [12] I. Szabó, G. Czakó, *Nat. Commun.* 6 (2015) 5972.
- [13] I. Szabó, G. Czakó, *J. Phys. Chem. A* 119 (2015) 3134.
- [14] D.A. Tasi, Z. Fábián, G. Czakó, *J. Phys. Chem. A* 122 (2018) 5773.
- [15] D.A. Tasi, Z. Fábián, G. Czakó, *Phys. Chem. Chem. Phys.* 21 (2019) 7924.
- [16] V. Tajti, G. Czakó, *J. Phys. Chem. A* 121 (2017) 2847.
- [17] Y.-T. Ma, X. Ma, A. Li, H. Guo, L. Yang, J. Zhang, W.L. Hase, *Phys. Chem. Chem. Phys.* 19 (2017) 20127.
- [18] P. Liu, D.Y. Wang, Y. Xu, *Phys. Chem. Chem. Phys.* 18 (2016) 31895.
- [19] P. Liu, J. Zhang, D.Y. Wang, *Phys. Chem. Chem. Phys.* 19 (2017) 14358.
- [20] B. Olasz, G. Czakó, *J. Phys. Chem. A* 123 (2019) 454.
- [21] Y. Li, D.Y. Wang, *Phys. Chem. Chem. Phys.* 20 (2018) 12106.
- [22] Y. Li, Y. Li, D.Y. Wang, *Phys. Chem. Chem. Phys.* 22 (2020) 12929.
- [23] I. Szabó, H. Telekes, G. Czakó, *J. Chem. Phys.* 142 (2015) 244301.
- [24] B. Olasz, I. Szabó, G. Czakó, *Chem. Sci.* 8 (2017) 3164.
- [25] A.Y. Dymarsky, K.N. Kudin, *J. Chem. Phys.* 122 (2005) 124103.
- [26] G. Czakó, *J. Phys. Chem. A* 116 (2012) 7467.
- [27] B. Olasz, G. Czakó, *Phys. Chem. Chem. Phys.* 21 (2019) 1578.
- [28] W.L. Hase, *Encyclopedia of Computational Chemistry*, Wiley, New York, 1998, pp. 399–407.
- [29] I. Szabó, B. Olasz, G. Czakó, *J. Phys. Chem. Lett.* 8 (2017) 2917.
- [30] B. Olasz, G. Czakó, *J. Phys. Chem. A* 122 (2018) 8143.